Synergistic Effects on Second Harmonic Generation of Hybrid CdSe−Au Nanoparticles

Ehud Shaviv and Uri Banin*

Institute of Chemistry and The Center for Nanoscience and Nanotechnology, The Hebrew University of Jerusalem, Jerusalem 91904, Israel

ABSTRACT Hybrid semiconductor−metal nanoparticles exhibit a combination of properties from the disparate components or even, more interestingly, synergetic properties which arise from the coupling between the two materials. In this work, we study the second harmonic generation (SHG) in CdSe−Au hybrid nanoparticles in comparison with their components, using the Hyper-Rayleigh scattering (HRS) method. Possible contribution of symmetry effects was studied by comparing symmetric two-sided gold-tipped CdSe nanodumbbells with asymmetric one-sided quantum dot−Au (QD−Au) hybrids. A simplistic view of a symmetry effect is disproved in this case by the experimental data, which shows an unexpected reduction in the SHG response in both cases, compared to the respective mixtures of Au and CdSe nanoparticles. For CdSe−Au hybrids with a long semiconductor rod segment, we find that the SHG response corresponds to a sum of the contributions from the semiconductor and the metal components. However, for QD−Au and smaller dumbbells, the SHG response is smaller than expected from a simple sum of the contribution from both components. This reduction is assigned to the effects related to the CdSe−Au interfacial region within these hybrids. A first plausible contribution to the reduction is the dephasing induced by the gold, leading to diminished SHG from the CdSe component. This reduced response of the semiconductor component is accompanied by reduced SHG from the gold component which is assigned to a partial change of the surface of the gold once an interface with CdSe is formed. These observations regarding the SHG response manifest the unique properties that arise from the combination of a semiconductor and a metal within one hybrid nanoparticle.

KEYWORDS: hybrid nanoparticles · quantum confinement effects · nonlinear optical properties · second harmonic generation

Advances in the synthesis of colloidal nanoparticles and in the understanding of their size, composition, and shape-dependent properties have enabled the preparation of new types of hybrid nanoparticles which combine two or more disparate materials, such as semiconductor/metal,[1−11] into one colloidal nanoparticle. In 2004, we reported a straightforward procedure enabling selective growth of gold tips onto the apexes of CdSe nanorods (NRs), resulting in the formation of dumbbell-shaped semiconductor/metal hybrids (nanodumbbells, NDBs).[1] The gold deposition method was later extended to other CdSe structures, enabling deposition of single gold tips onto quantum dots (QD−Au).[12] Such materials manifest a unique metal−semiconductor junction allowing for benchmark studies on the properties of nanoscale interfaces within a single nanoparticle.[13] As a result of this, the chemical and physical properties of hybrid nanoparticles are often different from those of the individual components comprising them. For example, regarding the optical properties, the absorption of the hybrid CdSe−Au NDBs is not a simple sum of the contributions of CdSe and Au separately. This may be attributed to mixing between the electronic states of the CdSe component and the Au NP (nanoparticles), resulting in a different density of states.[1] Furthermore, the emission from the NRs is significantly quenched once gold is grown on them, due to electron transfer from the conduction band of CdSe to the Au tip.[1,14,15] Similar modifications of the optical properties were reported for additional semiconductor− metal hybrid nanoparticles, such as CdS−Au.[2] To further explore the interaction between the semiconductor and the metal within the same nanoparticle, we study the nonlinear optical properties of these hybrids focusing on the second harmonic generation (SHG) process from CdSe−Au nanoparticles.

SHG arises from the second-order polarization of an entity induced by an optical electromagnetic field, E, as seen in the expansion of the response, P, as a power series of the excitation field:[16,17]

$$P = \alpha \cdot E + \beta : EE \qquad (1)$$

where α is the linear polarizability and β is the first-order hyperpolarizability that determines the extent of the second-order nonlinear response. SHG (frequency doubling) is forbidden for centrosymmetric

*Address correspondence to banin@chem.ch.huji.ac.il.

Received for review December 6, 2009 and accepted February 17, 2010.

Published online March 1, 2010.
10.1021/nn901778k

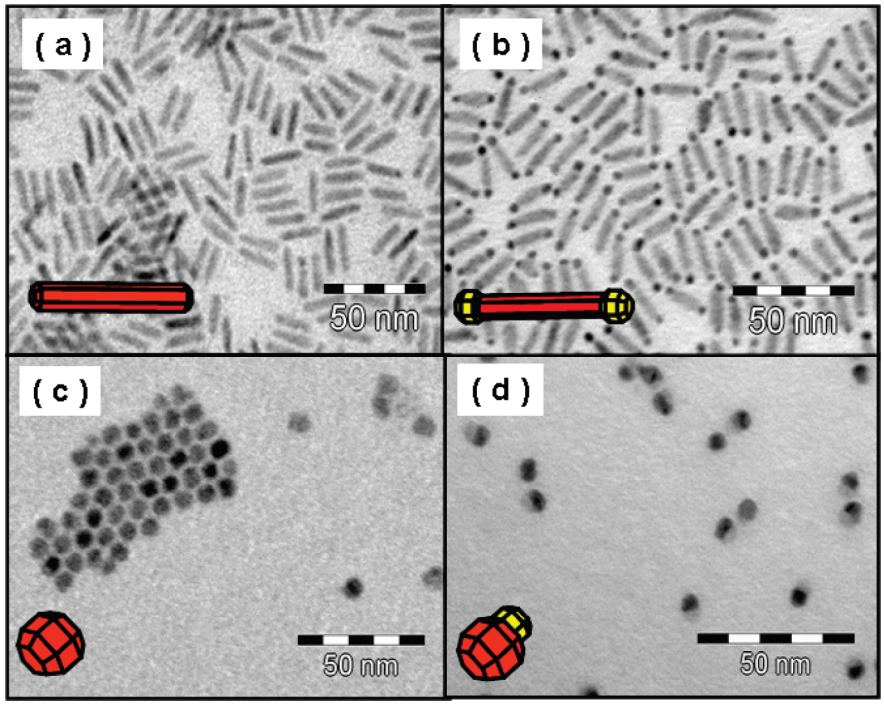

Figure 1. TEM images of (a) CdSe nanorods (21 × 5 nm), (b) CdSe−Au nanodumbbells (NDBs) grown from the nanorods in panel a (CdSe size: 17 × 5 nm, d_{Au} = 4 nm), (c) CdSe quantum dots (d = 7.5 nm), and (d) CdSe−Au QD−Au grown from the QDs in panel c (d_{CdSe}= 6.5 nm, d_{Au} = 4.3 nm). The length of the CdSe within the CdSe−Au nanodumbbells was measured as the distance between the two Au tips (scale bars are 50 nm).

media within the dipole approximation, and it is therefore strongly sensitive to the symmetry of the system.[16] Since centrosymmetry is inherently broken at an interface, SHG has been applied extensively as a probe to study processes on bulk surfaces or at interfaces between materials.[18−20] SHG from nanoparticles much smaller than the light wavelength represents a particularly interesting intermediate case between the molecular limit and the bulk. Simple symmetry considerations may suggest that symmetric shape will lead to cancellation of the SHG response.

As for SHG in noble metals nanoparticles (NPs), their symmetric crystal structure prohibits SHG originating from their internal medium. Studies on gold and copper NPs below 20 nm in diameter have shown that β is proportional to R^2 (R is the radius), consistent with a surface rather than volume response.[21,22] This observation along with a theoretical model by Dadap and co-workers[23,24] implies that the SHG process of small metal NPs arises from symmetry breaking at the surface related to deviations of the nanocrystals from a perfect spherical shape.[21,24] Polarization dependence measurements have demonstrated that, in small gold and copper NPs (R < 20 nm), the SHG process originates from an electric dipole scattering, rather than contributions from high-order multipoles.[21,22] Several theoretical and experimental studies have shown that noble metal NPs also exhibit a resonance effect which leads to an increase in the β value once the SHG frequency coincides with the plasmon frequency.[23−26]

As for semiconductor nanocrystals, several factors have been found to contribute to the SHG response from these systems.[27−33] Specifically, in the case of CdSe QDs, their wurtzite crystal structure is noncentrosymmetric and therefore the interior of the crystal itself can contribute to the SHG signal.[27,28] For small QDs (R < 1.7 nm), the β value per unit cell increases when the size is reduced. This behavior is in agreement with the two-level model developed for explaining the SHG of molecular systems with a charge transfer excited state.[27,28,34] Furthermore, as the size of the nanocrystal is reduced, surface contribution starts to play a role as well. This was confirmed by altering the surface cap ligands which led to a change in the SHG response of the nanocrystals.[29−31,35] Regarding the wavelength dependence of the SHG response, it was shown that for $Cd_xZn_{1-x}S$ QDs there is an increase in the value of β when the SHG is in resonance with the band gap transition.[31] This behavior is also in agreement with the two-level model mentioned above.[34] A recent study by Zyss and co-workers on coherent SHG scattering from single CdTe/CdS core/shell QDs revealed resonances in the SHG excitation spectrum around 970 nm, leading to increased SHG response at 485 nm, which is far above the band gap.[32] Furthermore, polarization analysis of the SHG response of these single nanoparticles resulted in patterns similar to those expected from their zinc blende unit cell structure.[32]

These earlier works on SHG from semiconductor and metal nanoparticles set the stage for the present investigation of synergetic effects on SHG from hybrid semiconductor/metal nanoparticles. We address several questions regarding the SHG response of Au−CdSe hybrid nanoparticles. First, we investigate possible contributions of symmetry effects by comparing the SHG response of symmetric two-sided gold-tipped NDBs with that of asymmetric one-sided tipped QD−Au hybrids. Second, we address the synergetic effects of the CdSe−Au interface by comparing the SHG response of the hybrid nanoparticles with that of a mixture of its components. Surprisingly, significant differences are found for the two cases, and the interpretation of this observation, directly pointing to synergic interactions, is discussed.

RESULTS AND DISCUSSION

Several types of hybrid Au−CdSe nanoparticles were studied, as seen in Figure 1, to allow for elucidat-

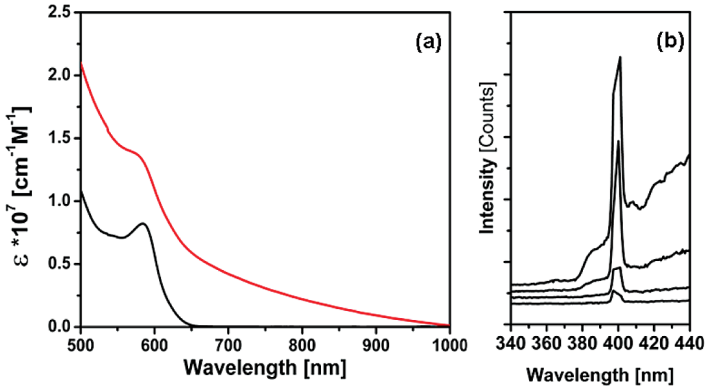

Figure 2. (a) Absorption spectra (calculated molar absorption coefficients plotted *versus* wavelength) are shown for a template of 43 × 4.5 nm CdSe nanorods before Au growth (black curve) and CdSe−Au nanodumbbells immediately after Au growth (red curve). The nanodumbbells' size after growth was smaller than the template (CdSe: 26 × 4.5 nm, d_{Au} = 4.4 nm). (b) Representative HRS spectra at various average excitation power in the range of 0.07−0.3 W are shown for these nanodumbbells. A well-defined peak is seen at the second harmonic frequency (400 nm). As the excitation increases, a significant multiphoton fluorescence background is observed. The spectra are offset for clarity.

ing the role of symmetry and size of the respective components on the SHG response. Prior to the SHG measurements, the molar absorption coefficients of the hybrid CdSe−Au nanoparticles were calculated based on the absorption change during Au growth (see Materials and Methods). Figure 2a shows the calculated molar absorption coefficients as a function of wavelength for the CdSe−Au NDB sample (CdSe: 25 × 4.5 nm, d_{Au} = 4.4 nm, red curve) and for the template CdSe NRs (43 × 4.5 nm, black curve) used for its growth. It is noticeable that, following Au deposition onto CdSe, a tail to the red side of the band gap appears and the features of the original NRs' absorbance are partially washed out, as reported previously.[1] Furthermore, the absorption coefficients at the visible range increase. For the sample shown in Figure 2a, at the peak of the first absorption feature, this increase is by a factor of 1.5. Similar measurements for other hybrid CdSe−Au samples have shown a similar increase of the absorption during Au growth, by a factor of 1.4−2 at the first absorption feature (see values in Table 1).

Regarding the SHG measurements, Figure 2b shows spectra collected from a CdSe−Au NDB solution for several representative average excitation powers. In all of the nanocrystal samples we have studied, a sharp SHG scattering signal at 400 nm, the doubled frequency, is seen. This signal is accompanied by a significant broad background signal. Furthermore, for gold nanoparticles and CdSe−Au samples which are exposed to high excitation levels, a tail at energies higher than the SHG peak starts to develop. Our measurements on samples that contained gold (either free Au NPs or CdSe−Au) show that this background signal, at energies lower than the SHG signal, manifest a dependence on the exciting laser intensity which is between quadratic and cubic. The same analysis for the background which developed at higher energies than the SHG peak has shown a cubic dependence. This implies that the background originates from emission as a result of a combination of two-photon and three-photon absorption processes originating from the gold and the semiconductor. In light of these observations, we note that previous studies have reported strong fluorescence signals induced by two-photon and three-photon absorption in noble metal nanoparticles[36,37] and semiconductor nanocrystals.[38−40] Since a significant background fluorescence signal was detected, special care was taken and all of the SHG signal intensities were obtained by subtracting the background from the original measured spectra, to extract exclusively the intensity of the sharp SHG peak.[41]

Hyper-Rayleigh Scattering (HRS) Measurements. Turning now to discuss the SHG response of the nanocrystals, the absolute β values for the nanocrystals were determined using the HRS method with the solvent serving as an internal reference.[42] For each sample, the intensity of the incoherent SHG scattering at 400 nm was measured as a function of the excitation intensity for the pure solvent and for several nanocrystal concentrations. The SHG signal intensity was corrected for losses due to internal absorption of the SHG signal. This correction uses Beer−Lambert law, based on the absorbance of the sample at 400 nm and the distance of the exciting beam from the cuvette edge. Figure 3 shows typical data analysis of SHG from CdSe−Au hybrid nanoparticle samples. The integrated intensity of the SHG signal, $I(2\omega)$, is plotted as a function of the excitation beam power, $I(\omega)$ (Figure 3 curves a−d). For each concentration, a good agreement to a parabolic fit is seen (solid lines), in accordance with the behavior expected for the incoherent HRS, described by the following equation:[42]

$$I(2\omega) = G(N_s\langle\beta^2\rangle_s + N_n\langle\beta^2\rangle_n)I(\omega)^2 \qquad (2)$$

G is a geometrical factor that also includes the contributions of local field factors. N_s and N_n are the concentration number density of the solvent (water) and the dissolved nanocrystals, respectively; $\langle\beta^2\rangle_s$ and $\langle\beta^2\rangle_n$ are the squares of the first-order hyperpolarizabilities of the solvent and the nanocrystals, respectively. The brackets denote the geometrical averaging of the tensor elements of β owing to the isotropic distribution of angular orientations of nanocrystals in the solution. The slopes of the parabolas (*i.e.*, the quadratic coefficients) are plotted as a function of the number density of the dissolved nanocrystals, as shown in the inset of Figure 3.

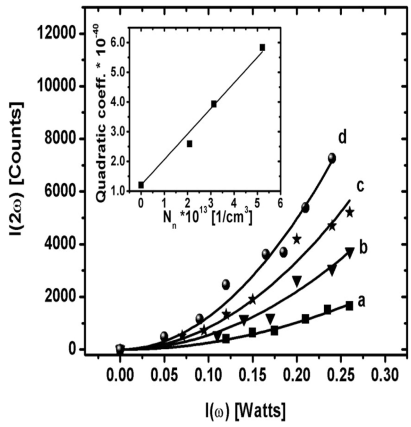

Figure 3. HRS data analysis for CdSe QD−Au (CdSe: 6.5 nm, d_{Au} = 4.3 nm). The intensity of $I(2\omega)$ *versus* $I(\omega)$ is plotted for three solutions with varying concentrations and for neat water: (a) neat water; (b) QD−Au concentration = 2.1 × 10^{13} cm^{-3}; (c) QD−Au concentration = 3.1 × 10^{13} cm^{-3}; (d) QD−Au concentration = 5.2 × 10^{13} cm^{-3}. The experimental data points are shown after correction for internal absorption of the SHG signal. The solid lines are quadratic fits for the dependence of $I(2\omega)$ on $I(\omega)$. Inset: quadratic coefficients are plotted *versus* the number density (concentration) of the nanocrystals. The plot is normalized based on the measured SHG response of the solvent (neat water). The $\langle\beta^2\rangle_n$ value of the nanocrystals was extracted from the slope of the linear fit (solid line) based on eq 2.

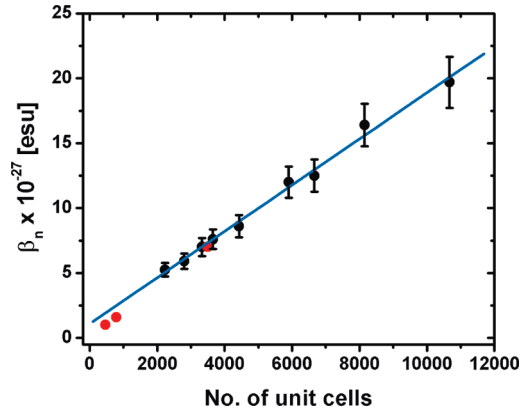

Figure 4. Size dependence of SHG response from CdSe nanorods is shown. The experimental $\langle\beta\rangle_n$ values, first hyperpolarizability per nanocrystal (black symbols), are plotted as a function of the calculated number of unit cells for nanorods of various dimensions (in growing $\langle\beta\rangle_n$ value order, the nanorod dimensions are 24 × 3.6, 32 × 3.5, 34 × 3.7, 20.5 × 5, 28 × 4.7, 43 × 4.5, 58 × 4, 42 × 5.2, and 55 × 5.2 nm). The data fit well to a linear dependence (solid line). On the basis of the slope, the value of the hyperpolarizability per unit cell, $\langle\beta\rangle_n$, is 2 × 10^{-30} esu. Three data points of $\langle\beta\rangle_n$ obtained experimentally for CdSe quantum dots in previous studies[27,29] (diameters = 4.6, 5.5, and 9 nm) (red symbols) exhibit a similar size dependence as the nanorods. A 10% error in the determined $\langle\beta\rangle_n$ values of the nanorods was taken into account.

A linear dependence is clearly seen as expected from eq 2. This plot is normalized to the value expected for neat water based on the calculated $\langle\beta\rangle_{water}$ value mentioned before. The square root of the slope of this plot is the absolute value of $\langle\beta_n\rangle$ of the nanocrystals as predicted from eq 2.

SHG of CdSe Nanorods. As a first step, we studied the SHG response of bare CdSe NRs. Measurements in the same manner described above were carried out for CdSe NRs with various dimensions, and for each NR sample, the value of $\langle\beta\rangle_n$ (first hyperpolarizability per nanocrystal) was extracted. In Figure 4, we plot these values for NR samples of different sizes (length range = 11−58 nm, diameter range = 3.5−5.5 nm) as a function of the calculated number of unit cells comprising the NRs (black symbols). In order to determine whether the shape of the nanocrystal has an effect on the $\langle\beta\rangle_n$ value, we add to this plot results for three spherical-shaped CdSe QDs (diameter = 4.6, 5.5, and 9 nm) obtained from previous studies[29,43] (red symbols). The number of unit cells of each sample was calculated based on the average dimensions of the nanocrystals, assuming cylindrical or spherical shape for NRs and QDs, respectively, and using the bulk density of hexagonal CdSe (d = 5.81 g/cm^3). For the NRs, a clear linear dependence between the number of unit cells (*i.e.*, the total volume of the nanocrystal) and the $\langle\beta\rangle_n$ value is observed. Furthermore, the results for QDs seem to fit well to the same linear trend (solid line), and therefore, we infer that these CdSe nanocrystals exhibit the same size dependence, regardless of their shape.

From the slope of the plot in Figure 4, we find that, for CdSe NRs and QDs, the value of β per unit cell is $\langle\beta\rangle_n \sim 2 \times 10^{-30}$ esu. Previous studies on the SHG of CdSe and CdS QDs have revealed a few possible contributions to the SHG process in these nanocrystals as mentioned above. For small CdSe nanocrystals, the surface and the surface ligands may have a significant contribution to the SHG response.[29] In this context, the 1D growth model suggested for CdSe NRs predicts that the surface of CdSe NRs is characterized by a ligand-free 001 Se-rich surface and an opposite 001 Cd-rich surface bound to ligands.[44] This surface structure introduces asymmetry to the "special" surfaces, which may increase the SHG response. However, for NRs with an aspect ratio of 3.3:1 and higher, less than 1/7 of the surface atoms occupy these special surfaces, and therefore, this surface asymmetry is not expected to have a significant effect on the SHG response. For larger CdSe QDs ($R > 2$ nm, more than 300 unit cells), the main contribution to the SHG process is from the interior media of the nanocrystal as exemplified in a previous study.[27] These CdSe nanocrystals are composed of a noncentrosymmetric unit cell (wurtzite), and therefore, as the volume of the nanocrystal increases, bulk-like volume dependence is anticipated because more Cd−Se bonds can contribute to the SHG response. The trend observed for NRs can be rationalized because all of the NRs have a relatively large volume (*i.e.*, more than 2000 unit cells) and therefore exhibit the same volume dependence as large QDs. Furthermore, we conclude that in this case the transformation from spherical to cylin-

drical nanocrystal shape does not affect the origin of the SHG process.

SHG of CdSe−Au Hybrid Nanoparticles. We now move on to discuss the SHG response of CdSe−Au semiconductor/metal hybrid nanoparticles. To understand the behavior of these hybrids, we have compared the response of NDBs to the response of mixtures of free Au NPs and CdSe NRs (keeping the mole ratio CdSe/Au 1:2 as in the NDBs). This approach provides a means to extract the net synergetic effect of the CdSe−Au combination within the NDBs *versus* the contribution of each separate component, with high accuracy. On the basis of eq 2, the slope of the measured quadratic coefficients as a function of the number density would yield the $\langle\beta^2\rangle$ value, referred to as the SHG response. The response for the mixture of CdSe NRs and Au NPs should follow the following behavior:

$$\text{slope} = \langle\beta^2\rangle_{\text{mix}} = \langle\beta^2\rangle_{\text{CdSe}} + 2\langle\beta^2\rangle_{\text{Au}} \qquad (3)$$

Since HRS is an incoherent scattering process, eq 3 is valid also for the hybrid CdSe−Au nanoparticles in case their SHG response would simply be a sum of contributions of the individual components. Figure 5 shows the SHG of the NDBs in comparison with SHG obtained from the mixture solutions for two different cases. Figure 5a shows a comparison of the SHG response of relatively long NDBs (CdSe 26 × 4.5 nm, Au diameter 4.4 nm, black circles) to the response of a mixture of CdSe NRs (24 × 4.5 nm) and Au NPs (diameter 4.3 nm) (red triangles). A linear fit to the data shows that both the mixture and the hybrid NDB sample exhibit a similar response ($\langle\beta^2\rangle_{\text{NDB}} = 1.15 \times 10^{-52}$ esu^2 and $\langle\beta^2\rangle_{\text{mix}} = 1.25 \times 10^{-52}$ esu^2, according to the slopes). However, for shorter NDBs, a different behavior is observed. Figure 5b shows a complementary experiment in which the SHG response of shorter NDBs (CdSe 14 × 3.7 nm, Au diameter 4.4 nm) was compared to the response of a mixture of CdSe NRs (11 × 3.8 nm) and Au NPs (diameter 4.3 nm). In this case, the slope from the linear fit for the NDBs is approximately 3 times smaller than the slope obtained for the mixture ($\langle\beta^2\rangle_{\text{NDB}} = 1.9 \times 10^{-53}$ esu^2, $\langle\beta^2\rangle_{\text{mix}} = 6.7 \times 10^{-53}$ esu^2, according to the slopes). From Figure 5, we infer that CdSe−Au NDBs exhibit a different SHG response as function of their size. While for the longer NDBs the SHG response seems to be a simple sum of contributions from both the CdSe and Au components, for shorter NDBs the SHG response is reduced significantly and it can no longer be considered as a simple sum of contributions from both components.

Aiming to corroborate this experimental observation, we measured SHG from several NDB samples of various dimensions and also one QD−Au hybrid sample. In order to understand the contribution of the gold tips, we also measured SHG from MUA-capped 4.3 nm Au NPs in aqueous solution (the size is close to the typical size of the tip in CdSe−Au hybrids and the surface capping ligand is also the same). Table 1 summarizes the results from all of these measurements. The experimental values of $\langle\beta\rangle$ obtained from each sample are given in column I in the table. For the Au NPs, a value of $\langle\beta\rangle = 6 \times 10^{-27}$ esu was obtained. Brevet and co-workers reported a larger value of $\langle\beta\rangle = 60 \times 10^{-27}$ esu for 5 nm Au NPs in water, excited at 1064 nm.[45] This order of magnitude difference between the results may be attributed to the plasmon resonance enhancement of the SHG effect at 532 nm, but we also note that we used a value of $\langle\beta\rangle$ for neat water that is 10 times smaller than the one used by Brevet and co-workers. Column II shows the experimental results from the comparison of the response of short and long NDBs to mixtures of their individual components presented in Figure 5.

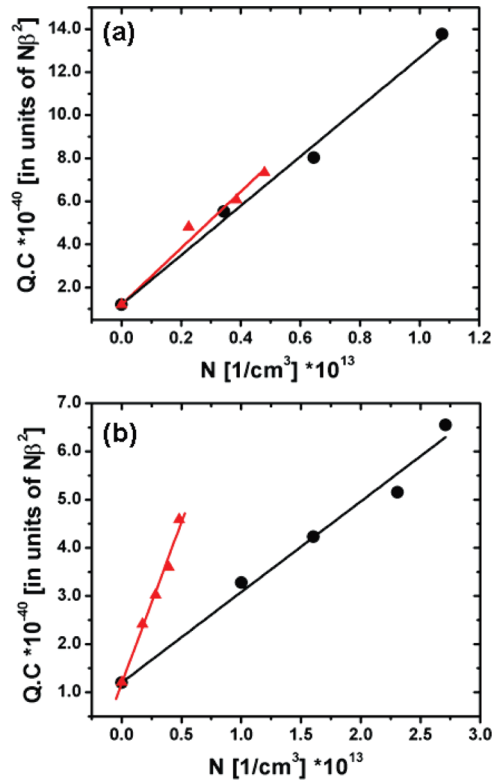

Figure 5. Comparison between the SHG response of CdSe−Au nanodumbbells (black circles) and corresponding mixtures of Au nanoparticles and CdSe nanorods with similar dimensions (red triangles). Quadratic coefficients (QC) are plotted *versus* the number density and fit to a linear trend as expected from eq 2. For the mixtures, we refer to the concentration of the nanorods. The intercept represents the contribution of neat solvent, water, which is used to normalize the SHG response. We compare two cases: (a) long nanodumbbells (CdSe: 26 × 4.5 nm, d_{Au} = 4.4 nm) compared to a mixture. The values of the slopes are 1.15 × 10^{-52} and 1.25 × 10^{-52} esu^2, respectively (solid lines); (b) shorter nanodumbbells (CdSe: 14 × 3.7 nm, d_{Au} = 4.4 nm) compared to a mixture. The values of the slopes are 1.9 × 10^{-53} and 6.7 × 10^{-53} esu^2, respectively (solid lines).

Next, we attempt to evaluate the contribution of the CdSe component to the SHG of the CdSe−Au hybrids. We assume this could be done since both large

TABLE 1. Summary of Results Obtained for Hybrid CdSe−Au and Au Nanoparticle SHG Response

	samples				measured values		calculations	
					I	II	III	IV
	sample type	CdSe size[a](nm)	Au size (nm)	molar absorption coefficient[b] (M^{-1} cm^{-1})	measured $\langle\beta\rangle_n \times 10^{-27}$ (esu)	measured $\langle\beta^2\rangle_{hybrid}/\langle\beta^2\rangle_{mixture}$[c]	CdSe $\langle\beta\rangle_n \times 10^{-27}$ (esu)	$\langle\beta^2\rangle_{hybrid}$/ calcd $\langle\beta^2\rangle_{mix}$[d]
1	Au NPs		4.3		6.0			
2	QD-Au	6.5	4.3	2.7×10^6	3.0		2.6	0.20
3	NDB	14×3.7	4.4	6×10^6	4.35	0.3	2.7	0.25
4	NDB	18×3.5	3.5	7.7×10^6	7.2		3.2	0.60
5	NDB	26×4.5	4.4	1.4×10^7	10.7	0.9	7	0.95
6	NDB	29×5	6	2×10^7	13.0		10	0.95

[a]The CdSe length in NDBs (nanodumbbells) is the average measured distance between the Au tips. [b]Value measured based on the change of absorbance at the location of the exciton peak immediately after Au growth on the CdSe. [c]The $\langle\beta^2\rangle$ mixture taken from the slope value obtained from measurements on mixtures of CdSe NRs and Au NPs. [d]The $\langle\beta^2\rangle$ mix value was calculated based on eq 3.

CdSe QDs and NRs exhibit a linear dependence of $\langle\beta\rangle$ on the volume as discussed above. This enables calculating the expected $\langle\beta\rangle$ value of the CdSe component within the hybrid nanoparticles. The calculated $\langle\beta\rangle_{CdSe}$ values are given in column III. In samples 2 and 3, QD−Au and short NDBs, respectively, the CdSe component has a similar volume and therefore close $\langle\beta\rangle_{CdSe}$ values were obtained. Samples 4−6 have larger CdSe content and correspondingly larger calculated values.

In column IV, we compare the measured response of the CdSe−Au hybrids ($\langle\beta^2\rangle_{hybrid}$) to the calculated response of a mixture of the two individual components ($\langle\beta^2\rangle_{mix}$). The response of the mixtures was calculated based on eq 3 (for QD−Au, contribution from only a single Au NP was considered). The values used for this calculation were the experimental $\langle\beta\rangle$ value obtained for Au NPs (6×10^{-27} esu) and the calculated $\langle\beta\rangle_{CdSe}$ values (given in column III). For samples 3 and 5, there is a similarity between the values shown in columns II and IV. Namely, for these samples, the calculated response of the mixture is close to the values obtained from the direct measurement of mixtures. This verifies that this method for calculation of the expected response of the mixture is indeed valid.

We move on to quantitatively compare the experimental results of the CdSe−Au hybrids (given in column I) to the calculated expected values for a mixture of their individual components. When we look at the values of samples 5 and 6 (in column IV), samples in which the CdSe component is relatively large, the response of the CdSe−Au hybrid is close to the expected response of a mixture of Au and CdSe nanocrystals ($\langle\beta^2\rangle_{hybrid}/\langle\beta^2\rangle_{mix} = 0.95$). However, for samples 2−4, the measured response of the hybrids is smaller than the expected response from a mixture ($\langle\beta^2\rangle_{hybrid}/\langle\beta^2\rangle_{mix} = 0.2-0.6$). Specifically, samples 2 and 3, QD−Au and short NDBs, respectively, exhibit similar values of $\langle\beta^2\rangle_{hybrid}/\langle\beta^2\rangle_{mix} = 0.2-0.25$. As mentioned before, in both of these samples, the CdSe component has the same volume.

It is noteworthy that unlike the NDBs, which are structures with a relatively high degree of symmetry, in the QD−Au sample (sample 2), the nanocrystal symmetry is inherently broken due to growth of a single Au tip (see Figure 1d for example). This might be expected to lead to enhanced SHG response. However, our experimental results show an opposite effect. Namely, the asymmetric CdSe−Au system shows a reduced response compared to the mixture. This therefore rules out the utility of simplistic symmetry considerations in assigning the SHG response of semiconductor/metal hybrids.

We now consider some of the factors which may lead to the observed reduction in the SHG response. First, the nonlinear polarization induced in a nanoparticle depends on the internal field within it. The internal field can be reduced or enhanced by the medium, according to the local field correction factor, which has the following form for metal and semiconductor nanostructures:[46,47]

$$f = \frac{3\varepsilon_m}{\varepsilon + 2\varepsilon_m} \tag{4}$$

where ε and ε_m denote the complex dielectric function of the metal and the surrounding medium, respectively. The power of the SHG signal from metal nanostructures then scales as[46]

$$P_{SHG} \propto |f(2\omega)|^2 |f^2(\omega)|^2 \tag{5}$$

where $f(2\omega)$ and $f(\omega)$ are the local field factors at the doubled frequency (400 nm) and at the fundamental frequency (800 nm), respectively. For the case of a mixture of CdSe and Au, both materials are within a water medium. In the other extreme, to examine what would be the effect of the different mediums in the hybrids, we consider the two limiting cases of a Au NP within CdSe, or *vice versa*, CdSe NP within Au. For both cases, the calculated local field factors are larger as compared to water medium (see Supporting Information). According to these calculations, the coupling between Au

and CdSe should result in an increase of the SHG response based on eq 5. Since this is not in agreement with the observed decrease in the SHG response, we conclude that local field factor cannot account for the observed reduction in the SHG response seen in some of the CdSe−Au hybrids.

Another source that may explain the observed reduction in SHG response is the degree of coherence of the detected SHG scattering from the samples. The linear dependence of $\langle\beta\rangle_n$ on the volume for CdSe NPs (see Figure 4) results from coherent addition of the signal from the unit cell. Similarly, a previous study that focused on the contribution of the surface to the SHG of CdSe QDs has also shown a coherent nature, such that the surface ligands contribute additively to the signal.[29] In the case of a coherent buildup of the SHG signal from a mixture of two components, the SHG intensity should be proportional to the second power of the summation of amplitudes of the SHG scattered fields from both components. Assuming such coherence within the hybrid nanoparticle, the SHG response for the QD−Au system (sample 2 in Table 1) could be described as

$$\langle\beta^2\rangle_{CdSe} + 2\langle\beta\rangle_{CdSe}\langle\beta\rangle_{Au} + \langle\beta^2\rangle_{Au} \quad (6)$$

The second term in eq 6 is an interference term, which may have a negative sign if $\langle\beta\rangle_{Au}$ is negative. In such a case, one might expect a partial reduction in the SHG response compared to the mixture of both individual components due to destructive interference. However, calculating the response under the assumption of a negative interference sign leads to a value which is 30% higher than the measured one (see Supporting Information). Similar calculation for the NDBs (sample 3 in Table 1) also leads to an estimate which is larger than the measured response (details appear in the Supporting Information). Therefore, we conclude that destructive interference cannot account for the observed reduction of SHG in the hybrids.

Moreover, we consider the possibility of damping of the SHG response of the semiconductor component within the hybrid NPs. The main origin of the SHG in CdSe nanocrystals is the unit cell.[27] The $\langle\beta\rangle$ value per unit cell in CdSe may be considered under the two-level model.[34] This model was developed to describe the $\langle\beta\rangle$ values of molecules at off resonance conditions, namely, when the SHG is far from the electronic transition and therefore damping due to electronic dephasing, optical transitions, or other processes is neglected.[48,49] Wang and coworkers have shown that the two-level model could be corrected taking into account damping due to electronic dephasing.[48,49] Their calculation for the two-level model with dephasing has shown that, when the damping rate constant is close in value to the frequency of the resonance, a significant reduction in $\langle\beta\rangle$ is expected. Under our experimental conditions, the resonance frequency (500−600 nm light, corresponding to the plasmon or the exciton wavelength range) is $\sim 3 \times 10^{15}$ s^{-1}. Since the SHG scattering is instantaneous, only damping close to such a time scale could lead to a reduction in the SHG response. Previous studies imply that dephasing within semiconductor nanocrystals at room temperature could occur on a time scale of a few femtoseconds.[50−53] Furthermore, it was hypothesized that the dephasing process could be sensitive to the environment of the nanocrystal.[54] In light of these findings, we consider the possibility of further significant damping (pure dephasing) induced within the CdSe component in proximity to the interface with the gold tips. The washing out and significant broadening of the absorption features once gold is deposited on CdSe support such an assumption.[1] Such a rapid damping process could also lead to a significant reduction in the CdSe unit cell contribution to SHG. This assignment gains support from the observation that the reduction of the measured SHG response compared to the calculated sum for the hybrid's components is most significant in the short CdSe−Au NDBs and the asymmetric QD−Au. In these, the CdSe−Au interface area is large relative to the CdSe volume, and therefore, the dephasing effect on CdSe SHG contribution would be most prominent. For larger CdSe−Au NDBs, the SHG signal is more closely represented as a simple sum of contributions of the components considering the relatively small CdSe−Au interface area compared to the CdSe volume.

Lastly, we reiterate that SHG in Au NPs is sensitive to the nature of the surface of the nanoparticle.[21−24,55,56] Even under the extreme assumption that the CdSe contribution to the SHG signal is completely diminished by dephasing effects, we still notice that the measured $\langle\beta\rangle_n$ values for samples 2 and 3 in Table 1 are smaller than the experimental value obtained for bare Au NPs (sample 1 in Table 1). These reduced values point to a reduction in the contribution from the surface of the Au component to the SHG signal, as well. We assign this reduction to the partial change in the surface of the gold component by formation of the Au/CdSe interface.

CONCLUSIONS

The main source of SHG from cylindrical-shaped CdSe NRs is a bulk-like contribution that is related to the nonlinear response of the Cd−Se bonds within the unit cell. This behavior is in agreement with that observed for CdSe QDs. The first-order hyperpolarizability, $\langle\beta\rangle$, in these nanocrystals exhibits therefore simple volume dependence. For hybrid CdSe−Au nanoparticles, two different behaviors are observed. First, both symmetric two-sided gold-tipped CdSe NDBs and asymmetric CdSe−Au hybrids exhibited reduction in the SHG response compared to appropriate mixtures of Au and CdSe

nanocrystals. This observation shows that simplistic symmetry considerations are not sufficient for analysis of the SHG response from such hybrids. Moreover, we find that for larger hybrid nanoparticles the SHG is a simple sum of contributions from the two components. However, hybrid CdSe−Au nanocrystals which contain a smaller CdSe component exhibit a surprising behavior, in which the SHG signal is significantly lower than the expected value from a mixture of the two components. This reduction effect is therefore most prominent in small hybrids for which the interfacial region of CdSe−Au is dominant. We suggest that dephasing effects of the gold domain on the proximal CdSe region can lead to such a reduction. Furthermore, the reduced ⟨β⟩ values imply that the contribution to the SHG signal from the surface of the Au nanoparticles within the hybrid is also decreased once an interface with CdSe is formed. These findings point to synergetic behavior arising from the unique combination of the semiconductor and metal domains within the hybrid nanoparticle.

MATERIALS AND METHODS

Sample Preparation: CdSe quantum dots and nanorods, capped with trioctylphosphine oxide (TOPO), hexadecylamine (HDA), and tetradecylphosphonic acid (TDPA), were synthesized in coordinating solvents using a high-temperature injection method as reported elsewhere.[57,58] The dimensions of the various samples were determined from transmission electron microscopy (TEM) images, based on statistics on more than 150 particles. The typical dimensions of the NRs were 10−60 nm for the length and 3.5−5.5 nm for the diameter. The typical standard deviations in size were 10% for both the length and the diameter of each sample. The diameter of the CdSe QD sample was 7.5 nm with a standard deviation of 10%.

Gold metal tips were deposited onto CdSe nanorods and QDs by adding a solution of $AuCl_3$, dissolved in toluene together with didodecyldimethylammonium bromide (DDAB) and dodecylamine (DDA) as previously reported.[1,12] The typical Au tip size according to size statistics was 4−6 nm with a standard deviation of 15%. The gold deposition reaction is also accompanied by a chemical etching process induced by the DDAB.[1] Consequently, the dimensions of the CdSe are reduced, leading to a loss of 35−50% of the volume of the CdSe component during the formation of the CdSe−Au hybrid as proven by size statistics.

All of the samples were transferred to an aqueous phase (Tris buffer, pH 9−10) by ligand exchange prior to the optical measurement. This step was taken in order to avoid thermal lensing effect, which was found to interfere with the SHG experiments. For a typical ligand exchange procedure, 25 mg of mercaptoundecanoic acid (MUA) was dissolved in 1 mL of aqueous solution of sodium bicarbonate (2 M, pH ∼9) and heated slightly to 70 °C. Next, the MUA solution was added to 1 mL of nanocrystals dissolved in chloroform (the optical density at the excitonic feature was 1−1.5). Next, 2 mL of Tris buffer (pH 9−10) was added to the mixture, which turned opaque. At this point, the solution was centrifuged and the upper aqueous phase of MUA-capped nanocrystals was extracted. The aqueous solutions were purified from access MUA by centrifugal filters (Millipore Amicon ultra-15) and afterward filtered again to minimize the presence of aggregates. For measurement on Au NPs, we used commercial aqueous solutions of citrate-coated Au NPs (Sigma-Aldrich G1402, average diameter 4.3 nm). The capping ligand was altered by adding MUA to the solutions.

SHG Optical Measurement: We have applied the Hyper-Rayleigh scattering (HRS) method in order to measure the absolute β value of the nanocrystals in solution.[42] During the measurements, a 1 cm long cuvette containing solutions of nanocrystals (in aqueous phase) with various concentrations was excited by a mode-locked Ti:sapphire laser at 810 nm (Coherent Mira). The pulse width was 120 fs, and the repetition rate was 76 MHz. The laser was vertically polarized, and the excitation power was attenuated by a variable neutral density filter. The laser beam with an average power in the range of 0.05−0.45W was focused to a tight spot of ∼100 μm. The scattered SHG signal at a doubled frequency was collected at a right angle, filtered with a short pass filter to suppress the fundamental excitation light, dispersed using a monochromator (Acton-150i), and detected with a liquid nitrogen cooled CCD (Princeton Instruments). It is noteworthy that samples that contained free Au NPs or CdSe−Au hybrids exhibited clear signs of thermal lensing effect (such as the laser beam "blooming" and reduction in the SHG signal). This is related to the red tail of the absorption of these nanocrystals, which extends to 800 nm, the excitation wavelength. In order to overcome these problem, two steps were taken. First, we used aqueous phase as a solvent instead of the original organic solvent (water has a higher heat capacity and hence reduced thermal lensing). In addition, all of the solutions were continuously circulated with a peristaltic pump during the measurements. The HRS measurements are conducted in "off resonance conditions", at 400 nm, namely, far from resonance with the band gap of the semiconductor (570−610 nm) or with the plasmon frequency of the gold NPs (∼510−520 nm).

Determining Nanocrystals Concentrations: The concentrations of all measured CdSe samples were calculated from the absorbance of the solutions based on Beer's law and their molar absorption coefficients (ε), which were obtained experimentally prior to the HRS measurements. Following a previous study[59] the ε values at the band edge for bare CdSe NRs were determined based on a combination of UV−vis absorption measurements and determination of the concentrations of the nanocrystals. This was achieved using ICP-AES (inductively coupled plasma atomic emission spectroscopy) elemental analysis along with size statistics from TEM imaging.[59] For CdSe QDs, the ε value at 350 nm was calculated assuming the same linear dependence on volume as exemplified by Bawendi and co-workers.[60] A combination of this value and the measured absorption spectra enabled us to determine the ε value at the band edge. For the determination of concentrations of CdSe−Au hybrids, a different approach was taken. For these nanocrystals, the ε value was calculated directly by comparing the absorption of the bare CdSe template sample to the absorption of the same sample immediately after gold growth solution has been added and Au growth has taken place. This simple calculation is based on the homogeneous growth of Au on all of the nanocrystals in the sample (as proven by TEM imaging) and on the fact that the number of nanocrystals in the solution has not changed during the reaction. For the determination of concentration of a 5 nm Au NP solution, a value of $\varepsilon = 1 \times 10^7\ cm^{-1}\ M^{-1}$ at the plasmon wavelength (520 nm) was used (based on the manufacturer data). This value was also verified by an ICP-AES measurement.

Determining the β Value of Water: An advantage of the HRS method is that the absolute value of β for the solute is obtained directly by using the solvent as an internal reference. In order to extract the value of β for water, we have measured the intensity of $I(2\omega)$ as function of $I(\omega)$ for toluene and water. The curves were fit to a parabolic dependence, and their quadratic coefficients were determined. These quadratic coefficients were used to calculate the β of water, based on the known value for toluene at 800 nm ($\langle\beta\rangle_{toluene} = 0.25 \times 10^{-30}$ esu)[27] and using the following equation:[61,62]

$$\beta_{water} = \frac{[f^2(\omega)f(2\omega)]_{toluene}}{[f^2(\omega)f(2\omega)]_{water}} \frac{n(2\omega)_{water}}{n(2\omega)_{toluene}} \sqrt{\frac{QC_{water}N_{toluene}}{QC_{toluene}N_{water}}} \beta_{toluene} \quad (7)$$

where $f(\omega)$ and $f(2\omega)$ are the local field factors at the fundamental and the doubled frequency, which are included based on the Lorentz correction factor;[61,62] $n(2\omega)$ refers to the refractive index at 400 nm, which influences the SHG signal collection efficiency.[62] QC is the experimental quadratic coefficients extracted from the parabolic curves, and N is the number density of each solvent (in cm^{-3}). From the calculation in eq 7, we deduce a value of $\langle\beta\rangle_s = 0.06 \times 10^{-30}$ esu for pure water at $\lambda = 800$ nm, which is an order of magnitude smaller than the value reported for water in previous studies of SHG from metal nanoparticles at $\lambda = 1064$ nm ($\langle\beta\rangle_s = 0.56 \times 10^{-30}$ esu).[45,63,64] A comparison between the quadratic SHG response of pure water and Tris buffer, which was used as the solvent in practice, has shown little difference, and therefore, we have used pure water as the reference.

Acknowledgment. Partial funding by the Nanosci ERA-Net program under the program single-nanohybrid and by the Farkas center for light induced processes is acknowledged. The authors thank Dr. Yitzhak Shweky and Asaf Salant for their assistance with TEM imaging and sample preparation, and Dr. Dan Oron for helpful discussion. U.B. wishes to thank the Alfred and Erica Larisch Memorial Chair in Solar Energy.

Supporting Information Available: Local field factors calculations for Au/water, Au/CdSe, CdSe/water, CdSe/Au; calculations of the expected response in case of coherence between Au and CdSe within the CdSe−Au hybrids. This material is available free of charge *via* the Internet at http://pubs.acs.org.

REFERENCES AND NOTES

1. Mokari, T.; Rothenberg, E.; Popov, I.; Costi, R.; Banin, U. Selective Growth of Metal Tips onto Semiconductor Quantum Rods and Tetrapods. *Science* **2004**, *304*, 1787–1790.
2. Saunders, A. E.; Popov, I.; Banin, U. Synthesis of Hybrid CdS-Au Colloidal Nanostructures. *J. Phys. Chem. B* **2006**, *110*, 25421–25429.
3. Menagen, G.; Mocatta, D.; Salant, A.; Popov, I.; Dorfs, D.; Banin, U. Selective Gold Growth on CdSe Seeded CdS Nanorods. *Chem. Mater.* **2008**, *20*, 6900–6902.
4. Elmalem, E.; Saunders, A. E.; Costi, R.; Salant, A.; Banin, U. Growth of Photocatalytic CdSe−Pt Nanorods and Nanonets. *Adv. Mater.* **2008**, *20*, 4312–4317.
5. Mokari, T.; Aharoni, A.; Popov, I.; Banin, U. Diffusion of Gold into InAs Nanocrystals. *Angew. Chem., Int. Ed.* **2006**, *45*, 8001–8005.
6. Habas, S. E.; Yang, P.; Mokari, T. Selective Growth of Metal and Binary Metal Tips on CdS Nanorods. *J. Am. Chem. Soc.* **2008**, *130*, 3294–3295.
7. Wood, A.; Giersig, M.; Mulvaney, P. Fermi Level Equilibration in Quantum Dot−Metal Nanojunctions. *J. Phys. Chem. B* **2001**, *105*, 8810–8815.
8. Cozzoli, P. D.; Pellegrino, T.; Manna, L. Synthesis, Properties and Perspectives of Hybrid Nanocrystal Structures. *Chem. Soc. Rev.* **2006**, *35*, 1195–1208.
9. Shi, W.; Zeng, H.; Sahoo, Y.; Ohulchanskyy, T. Y.; Ding, Y.; Wang, Z. L.; Swihart, M.; Prasad, P. N. A General Approach to Binary and Ternary Hybrid Nanocrystals. *Nano Lett.* **2006**, *6*, 875–881.
10. Dukovic, G.; Merkle, M. G.; Nelson, J. H.; Hughes, S. M.; Alivisatos, A. P. Photodeposition of Pt on Colloidal CdS and CdSe/CdS Semiconductor Nanostructures. *Adv. Mater.* **2008**, *20*, 4306–4311.
11. Lee, J. S.; Shevchenko, E. V.; Talapin, D. V. Au−PbS Core−Shell Nanocrystals: Plasmonic Absorption Enhancement and Electrical Doping *via* Intra-particle Charge Transfer. *J. Am. Chem. Soc.* **2008**, *130*, 9673–9675.
12. Mokari, T.; Sztrum, C. G.; Salant, A.; Rabani, E.; Banin, U. Formation of Asymmetric One-Sided Metal-Tipped Semiconductor Nanocrystal Dots and Rods. *Nat. Mater.* **2005**, *4*, 855–863.
13. Steiner, D.; Mokari, T.; Banin, U.; Millo, O. Electronic Structure of Metal−Semiconductor Nanojunctions in Gold CdSe Nanodumbbells. *Phys. Rev. Lett.* **2005**, *95*, 056805.
14. Costi, R.; Saunders, A. E.; Elmalem, E.; Salant, A.; Banin, U. Visible Light-Induced Charge Retention and Photocatalysis with Hybrid CdSe−Au Nanodumbbells. *Nano Lett.* **2008**, *8*, 637–641.
15. Costi, R.; Cohen, G.; Salant, A.; Rabani, E.; Banin, U. Electrostatic Force Microscopy Study of Single Au−CdSe Hybrid Nanodumbbells: Evidence for Light-Induced Charge Separation. *Nano Lett.* **2009**, *9*, 2031–2039.
16. Shen, Y. R. *the Principles of Nonlinear Optics*; Wiley: New York, 1984.
17. Chemla, D. S.; Zyss, J. *Nonlinear Optical Properties of Organic Molecules and Crystals*; Academic Press: Orlando, FL, 1987.
18. Williams, C. T.; Beattie, D. A. Probing Buried Interfaces with Non-linear Optical Spectroscopy. *Surf. Sci.* **2002**, *500*, 545–576.
19. Richmond, G. L.; Robinson, J. M.; Shannon, V. L. 2nd Harmonic-Generation Studies of Interfacial Structure and Dynamics. *Prog. Surf. Sci.* **1988**, *28*, 1–70.
20. Eisenthal, K. B. Liquid Interfaces Probed by Second-Harmonic and Sum-Frequency Spectroscopy. *Chem. Rev.* **1996**, *96*, 1343–1360.
21. Nappa, J.; Revillod, G.; Russier-Antoine, I.; Benichou, E.; Jonin, C.; Brevet, P. F. Electric Dipole Origin of the Second Harmonic Generation of Small Metallic Particles. *Phys. Rev. B* **2005**, *71*, 165407.
22. Chandra, M.; Indi, S. S.; Das, P. K. Depolarized Hyper-Rayleigh Scattering from Copper Nanoparticles. *J. Phys. Chem. C* **2007**, *111*, 10652–10656.
23. Dadap, J. I.; Shan, J.; Eisenthal, K. B.; Heinz, T. F. Second-Harmonic Rayleigh Scattering from a Sphere of Centrosymmetric Material. *Phys. Rev. Lett.* **1999**, *83*, 4045–4048.
24. Dadap, J. I.; Shan, J.; Heinz, T. F. Theory of Optical Second-Harmonic Generation from a Sphere of Centrosymmetric Material: Small-Particle Limit. *J. Opt. Soc. Am. B* **2004**, *21*, 1328–1347.
25. Russier-Antoine, I.; Jonin, C.; Nappa, J.; Benichou, E.; Brevet, P. F. Wavelength Dependence of the Hyper Rayleigh Scattering Response from Gold Nanoparticles. *J. Chem. Phys.* **2004**, *120*, 10748–10752.
26. Abid, J. P.; Nappa, J.; Girault, H. H.; Brevet, P. F. Pure Surface Plasmon Resonance Enhancement of the First Hyperpolarizability of Gold Core−Silver Shell Nanoparticles. *J. Chem. Phys.* **2004**, *121*, 12577–12582.
27. Jacobsohn, M.; Banin, U. Size Dependence of Second Harmonic Generation in CdSe Nanocrystal Quantum Dots. *J. Phys. Chem. B* **2000**, *104*, 1–5.
28. Santos, B. S.; Pereira, G. A. L.; Petrov, D. V.; Donega, C. D. First Hyperpolarizability of CdS Nanoparticles Studied by Hyper-Rayleigh Scattering. *Opt. Commun.* **2000**, *178*, 187–192.
29. Eilon, M. J.; Mokari, T.; Banin, U. Surface Exchange Effect on Hyper Rayleigh Scattering in CdSe Nanocrystals. *J. Phys. Chem. B* **2001**, *105*, 12726–12731.
30. Landes, C.; Braun, M.; El-Sayed, M. A. The Effect of Surface Adsorption on the Hyper-Rayleigh Scattering of Large and Small CdSe Nanoparticles. *Chem. Phys. Lett.* **2002**, *363*, 465–470.
31. Petrov, D. V.; Santos, B. S.; Pereira, G. A. L.; de Mello Donega, C. Size and Band-Gap Dependences of the First Hyperpolarizability of $Cd_xZn_{1-x}S$ Nanocrystals. *J. Phys. Chem. B* **2002**, *106*, 5325–5334.
32. Zielinski, M.; Oron, D.; Chauvat, D.; Zyss, J. Second-Harmonic Generation from a Single Core/Shell Quantum Dot. *Small* **2009**, *5*, 2835–2840.
33. Son, D. H.; Wittenberg, J. S.; Banin, U.; Alivisatos, A. P. Second Harmonic Generation and Confined Acoustic Phonons in Highly Excited Semiconductor Nanocrystals. *J. Phys. Chem. B* **2006**, *110*, 19884–19890.
34. Oudar, J. L.; Chemla, D. S. Hyperpolarizabilities of Nitroanilines and Their Relations to Excited-State Dipole-Moment. *J. Chem. Phys.* **1977**, *66*, 2664–2668.

35. Zhang, Y.; Wang, X.; Ma, M.; Fu, D. G.; Gu, N.; Liu, J. Z.; Lu, Z. H.; Ma, Y.; Xu, L.; Chen, K. J. Influence of Surface-Capping Molecule Exchange on the Hyper-Rayleigh Scattering of CdS Nanoparticles. *Appl. Surf. Sci.* **2003**, *205*, 256–261.
36. Farrer, R. A.; Butterfield, F. L.; Chen, V. W.; Fourkas, J. T. Highly Efficient Multiphoton-Absorption-Induced Luminescence from Gold Nanoparticles. *Nano Lett.* **2005**, *5*, 1139–1142.
37. Xiao, S.; Gong, H. M.; Su, X. R.; Han, J. B.; Han, Y. B.; Chen, M. T.; Wang, Q. Q. Two- and Three-Photon Luminescence of Au Nanoparticles and Resonant Energy Transfer from CdSe Quantum Dots. *J. Phys. Chem. C* **2007**, *111*, 10185–10189.
38. Rothenberg, E.; Ebenstein, Y.; Kazes, M.; Banin, U. Two-Photon Fluorescence Microscopy of Single Semiconductor Quantum Rods: Direct Observation of Highly Polarized Nonlinear Absorption Dipole. *J. Phys. Chem. B* **2004**, *108*, 2797–2800.
39. Larson, D. R.; Zipfel, W. R.; Williams, R. M.; Clark, S. W.; Bruchez, M. P.; Wise, F. W.; Webb, W. W. Water-Soluble Quantum Dots for Multiphoton Fluorescence Imaging *In Vivo*. *Science* **2003**, *300*, 1434–1436.
40. Schmidt, M. E.; Blanton, S. A.; Hines, M. A.; GuyotSionnest, P. Size-Dependent Two-Photon Excitation Spectroscopy of CdSe Nanocrystals. *Phys. Rev. B* **1996**, *53*, 12629–12632.
41. The background under the SHG peak was obtained by interpolation of the signal on both sides of the peak based on a third degree polynomial fit. This fit was subtracted from the measured signal to obtain the corrected SHG intensity.
42. Clays, K.; Persoons, A. Hyper-Rayleigh Scattering in Solution with Tunable Femtosecond Continuous-Wave Laser Source. *Rev. Sci. Instrum.* **1994**, *65*, 2190–2194.
43. Eilon, M. J.; Mokari, T.; Banin, U. Surface Exchange Effect on Hyper Rayleigh Scattering in CdSe Nanocrystals. *J. Phys. Chem. B* **2001**, *105*, 12726–12731.
44. Peng, Z. A.; Peng, X. Mechanisms of the Shape Evolution of CdSe Nanocrystals. *J. Am. Chem. Soc.* **2001**, *123*, 1389–1395.
45. Galletto, P.; Brevet, P. F.; Girault, H. H.; Antoine, R.; Broyer, M. Size Dependence of the Surface Plasmon Enhanced Second Harmonic Response of Gold Colloids: Towards a New Calibration Method. *Chem. Commun.* **1999**, 581–582.
46. Maier, S. A. *Plasmonics: Fundamentals and Applications*, 1st ed.; Springer: New York, 2007.
47. Moreels, I.; Lambert, K.; Smeets, D.; De Muynck, D.; Nollet, T.; Martins, J. C.; Vanhaecke, F.; Vantomme, A.; Delerue, C.; Allan, G.; Hens, Z. Size-Dependent Optical Properties of Colloidal PbS Quantum Dots. *ACS Nano* **2009**, *3*, 3023–3030.
48. Wang, C. H.; Woodford, J. N.; Jen, A. K. Y. Measurements of the First Hyperpolarizabilities of Thiophene-Based Charge-Transfer Chromophores with Hyper-Rayleigh Scattering at 1064 and 1907 nm. *Chem. Phys.* **2000**, *262*, 475–487.
49. Wang, C. H. Effects of Dephasing and Vibronic Structure on the First Hyperpolarizability of Strongly Charge-Transfer Molecules. *J. Chem. Phys.* **2000**, *112*, 1917–1924.
50. Mittleman, D. M.; Schoenlein, R. W.; Shiang, J. J.; Colvin, V. L.; Alivisatos, A. P.; Shank, C. V. Quantum-Size Dependence of Femtosecond Electronic Dephasing and Vibrational Dynamics in CdSe Nanocrystals. *Phys. Rev. B* **1994**, *49*, 14435–14447.
51. Fernee, M. J.; Jensen, P.; Rubinsztein-Dunlop, H. Origin of the Large Homogeneous Line Widths Obtained from Strongly Quantum Confined PbS Nanocrystals at Room Temperature. *J. Phys. Chem. C* **2007**, *111*, 4984–4989.
52. Kamisaka, H.; Kilina, S. V.; Yamashita, K.; Prezhdo, O. V. *Ab Initio* Study of Temperature- and Pressure Dependence of Energy and Phonon-Induced Dephasing of Electronic Excitations in CdSe and PbSe Quantum Dots. *J. Phys. Chem. C* **2008**, *112*, 7800–7808.
53. Woggon, U.; Portune, M. Femtosecond Dephasing in CdS Quantum Dots Determined by Nondegenerate 4-Wave-Mixing. *Phys. Rev. B* **1995**, *51*, 4719–4722.
54. Ikezawa, M.; Masumoto, Y. Ultranarrow Homogeneous Broadening of Confined Excitons in Quantum Dots: Effect of the Surrounding Matrix. *Phys. Rev. B* **2000**, *61*, 12662–12665.
55. Russier-Antoine, I.; Bachelier, G.; Sabloniere, V.; Duboisset, J.; Benichou, E.; Jonin, C.; Bertorelle, F.; Brevet, P. F. Surface heterogeneity in Au−Ag Nanoparticles Probed by Hyper-Rayleigh Scattering. *Phys. Rev. B* **2008**, *78*, 035436.
56. Kim, Y. J.; Johnson, R. C.; Li, J. G.; Hupp, J. T.; Schatz, G. C. Synthesis, Linear Extinction, and Preliminary Resonant Hyper-Rayleigh Scattering Studies of Gold−Core/Silver−Shell Nanoparticles: Comparisons of Theory and Experiment. *Chem. Phys. Lett.* **2002**, *352*, 421–428.
57. Peng, X. G.; Manna, L.; Yang, W. D.; Wickham, J.; Scher, E.; Kadavanich, A.; Alivisatos, A. P. Shape Control of CdSe Nanocrystals. *Nature* **2000**, *404*, 59–61.
58. Mokari, T.; Banin, U. Synthesis and Properties of CdSe/ZnS Core/Shell Nanorods. *Chem. Mater.* **2003**, *15*, 3955–3960.
59. Shaviv, E.; Salant, A.; Banin, U. Size Dependence of Molar Absorption Coefficients of CdSe Semiconductor Quantum Rods. *ChemPhysChem* **2009**, *10*, 1028–1031.
60. Leatherdale, C. A.; Woo, W. K.; Mikulec, F. V.; Bawendi, M. G. On the Absorption Cross Section of CdSe Nanocrystal Quantum Dots. *J. Phys. Chem. B* **2002**, *106*, 7619–7622.
61. Prasad, P. N.; Williams, D. J. *Introduction to Nonlinear Optical Effects in Molecules and Polymers*; Wiley: New York 1991.
62. Lakowicz, J. R. *Priniciples of Fluorescence Spectroscopy*, 2nd ed.; Kluwer Academic/Plenum Publishers: New York, 1999.
63. Vance, F. W.; Lemon, B. I.; Hupp, J. T. Enormous Hyper-Rayleigh Scattering from Nanocrystalline Gold Particle Suspensions. *J. Phys. Chem. B* **1998**, *102*, 10091–10093.
64. Russier-Antoine, I.; Huang, J.; Benichou, E.; Bachelier, G.; Jonin, C.; Brevet, P. F. Hyper Rayleigh Scattering of Protein-Mediated Gold Nanoparticles Aggregates. *Chem. Phys. Lett.* **2008**, *450*, 345–349.